Colloids and Surfaces B: Biointerfaces 183 (2019) 110436

Contents lists available at ScienceDirect

Colloids and Surfaces B: Biointerfaces

journal homepage: www.elsevier.com/locate/colsurfb

Mechanistic study of colorimetric and absorbance sensor developed for trivalent yttrium (Y^{3+}) using chlortetracycline-functionalized silver nanoparticles

Gajanan Ghodake[a], Surendra Shinde[a], Rijuta Ganesh Saratale[b], Avinash Kadam[b], Ganesh Dattatraya Saratale[c], Dae-Young Kim[a,*]

[a] Department Biological and Environmental Science, Dongguk University-Seoul, Ilsandong-gu, 10326, Goyang-si, Gyeonggi-do, Republic of Korea
[b] Research Institute of Biotechnology and Medical Converged Science, Dongguk University-Seoul, Ilsandong-gu, Goyang-si, Gyeonggi-do, 10326, Republic of Korea
[c] Department of Food Science and Biotechnology, Dongguk University-Seoul, Ilsandong-gu, Goyang-si, Gyeonggi-do, 10326, Republic of Korea

ARTICLE INFO

Keywords:
Chlortetracycline
Silver nanoparticles
Colorimetric
High sensitivity
Radioactive metals
Yttrium
Lanthanides

ABSTRACT

The presence of hazardous, radioactive, and rare earth metal such as yttrium (Y^{3+}) in water poses a serious health concern to the public health, thus, exploring novel Y^{3+}-binding molecules and colorimetric indicators are desired. Chlortetracycline (CTC)-functionalized silver nanoparticles (AgNPs–CTC) were synthesized, purified by centrifugation and then characterized by UV–vis spectroscopy, XPS, XRD, and HR-TEM. Functionalization of AgNPs with CTC molecules enabled the rapid and sensitive detection of trivalent yttrium ion (Y^{3+}). A decrease in the intensity of the original surface plasmon resonance peak at 420 nm was observed within the fraction of a min, with the simultaneous appearance of a new peak at a longer wavelength (540 nm); thus, a novel colorimetric and ratiometric absorbance probe was achieved. The free-O-containing moieties of CTC on the AgNPs surface coordinate with Y^{3+}. Thus, CTC molecules led to the bridging of the AgNPs and subsequent aggregation. A good linear relationship (R^2 = 0.933) in the range of 18 to 243 nM for Y^{3+} was observed, and the limit of detection (LOD) for ratiometric results was approximately 57.7 nM. The AgNPs–CTC sensor exhibited better colorimetric performance in terms of excellent sensitivity, LOD, and rapid formation of the AgNPs-CTC complex towards Y^{3+}. The Y^{3+} spiked water samples from different sources and fetal bovine serum suggest that the developed method is practically useful and essentially portable for on-site monitoring. The AgNPs–CTC sensor can be also applied as a common colorimetric indicator for the detection of trace levels of Y^{3+} and lanthanides.

1. Introduction

Facile detection of metal ions is of interest with high sensitivity, basically in aqueous media, is an important research area. Over the past several decades, research into the applications and biological significance of yttrium-compound based biomedical products has increased dramatically [1,2]. It is one of the important radioisotopes frequently released from radioactive waste into the environment [3]. Yttrium (Y^{3+}) are quite hazardous and non-biodegradable; thus, they must be detected and safely removed from polluted streams. Similarly, increased use of lanthanides in catalysis, fertilizer, and medical diagnosis, it has raised serious concerns over their potential in pollution and deserves new methods detection of trace levels [4]. Traditional methods such as inductively coupled plasma atomic emission spectrometry [5], and inductively coupled plasma mass spectrometry (ICP-MS) [6] have typically been used to detect Y^{3+}. Also, some fluorescence sensors for Y^{3+} have also been reported, that shown molecular recognition capability for the Y^{3+} metal ions [7,8]. In addition, only a limited number of Y^{3+} samples have thus far been examined [9]. As such, the developments of more effective, rapid, and selective colorimetric or spectrophotometric methods with the capability to detect Y^{3+} ions with nanomolar-level sensitivity are needed. To the best of our knowledge, the present work is the first report on the sensitive colorimetric detection and determination of Y^{3+} using chlortetracycline (CTC)-functionalized silver nanoparticles (AgNPs–CTC) with a dependable and rapid absorbance response.

Organic compounds with electron-donor functionality are important in analytical chemistry, where they participate in environmental, biological, medicinal, and organometallic coordination reactions for binding with metal ions [10]. Members of the tetracycline class of

* Corresponding author.
E-mail address: sbpkim@dongguk.edu (D.-Y. Kim).

https://doi.org/10.1016/j.colsurfb.2019.110436
Received 19 June 2019; Received in revised form 6 August 2019; Accepted 8 August 2019
Available online 09 August 2019

antibiotics have hydrophilic functional groups, are readily water-soluble, and acts as a chelating agent, particularly for trivalent metal ions [11]. The motivation of the current study is to integrate previous observations concerning possible interactions between CTC and radioactive Y^{3+} by simply using CTC functionalized AgNPs. This study demonstrates that CTC readily caps onto the surface of AgNPs, thereby providing not only long-term stability in the absence of other organic compounds or aggressive reagents but also acts as a molecular platform for the quantitative determination of Y^{3+} ions. However, such ligand coordination chemistry has yet to be explored as a colorimetric and absorbance sensor for Y^{3+}.

In the present work, we developed a colorimetric sensor to detect Y^{3+} concentrations at the nanomolar level using AgNPs–CTC. The newly developed colorimetric method is based on the complexation of CTC with Y^{3+} in a weakly acidic to weakly basic medium ($5 \leq pH \leq 9.0$) at ambient temperature. The absorbance of the resultant suspension was orange and red-colored after AgNPs–CTC binding with Y^{3+} and it was measured at two different λ_{max} values of 420 and 540 nm. In this sensor, the absorbance band of the AgNPs–CTC ligand pairs well with the excitation energy of Y^{3+}, which leads to a high energy transfer from the CTC to the Y^{3+}, induces aggregation and red-shift of the absorption peak. Y^{3+} binds with CTC through a potential O-containing moiety; CTC thus acts as a chelating ligand, where the absorbance intensity of the AgNPs is influenced by the concentration of Y^{3+} ions. The AgNPs–CTC sensor was also used to detect Y^{3+} in spiked samples such as real water samples from different sources and fetal bovine serum; the obtained results were satisfactory and sensible.

2. Experimental details

2.1. Materials and reagents

Silver nitrate ($AgNO_3$) was obtained from Sigma-Aldrich Chemical Co. (United States). Yttrium salt and NaOH were obtained from Dae Jung Chemical Co. (South Korea). Chlortetracycline (CTC) was obtained from MB Cell Co. (South Korea). All metal salts were purchased either from Dae Jung Chemical Co. (South Korea), Kanto Chemical Co. (Tokyo, Japan), or Nacalai Tesque Inc. (Kyoto, Japan). All aqueous reagent solutions and AgNPs dispersions were prepared using nanopure water (Thermo Scientific, South Korea).

2.2. Synthesis of AgNPs-CTC

CTC is the first tetracycline antibiotics isolated from an organism named *Streptomyces aureofaciens*. In veterinary medicine, CTC is being used to treat conjunctivitis and infected wounds in dogs, cats, and horses. In this study, we used CTC as a reducing and stabilizing agent for the synthesis of AgNPs-CTC in aqueous solution by biochemical reduction of $AgNO_3$. This green nano-synthesis process was carried out in 15 mL plastic tubes rinsed with copious amounts of nanopure water. A mixture of 3 mL of a 3 mM solution of CTC with 0.2 mL of 1.0 M NaOH and 4.8 mL nanopure water was incubated at one of four different temperatures (20, 40, 60, and 80 °C). Finally, 2 mL of a 20 mM solution of $AgNO_3$ was mixed and incubated at temperatures as mentioned above. The color of the incubated solutions of all of the samples rapidly changed from colorless to dark yellow and then to dark **brown.**After the addition of 2 mL of the 20 mM $AgNO_3$ solution, aliquots were collected from the reaction at different time intervals for 300 min. The AgNP-CTC aliquots were then analyzed by ultraviolet-visible (UV–vis) spectrophotometry (Optizen 2120) in the wavelength range from 300 to 800 nm. The AgNP-CTC solutions for UV–vis spectroscopy were diluted by the addition of 0.05 mL of the reaction solution into 1.95 mL of nanopure water. The evolution of the UV–vis spectrum and absorbance of each sample were plotted vs. time (from 10 to 300 min) to characterize the optical properties and productivity based on the λ_{max} values.

2.3. AgNPs-CTC purification

The AgNPs-CTC solution prepared at 80 °C was centrifuged at 12,000 rpm for 15 min. A pellet of the ultracentrifuge AgNPs was dispersed in nanopure water. The removal of excess NaOH, $AgNO_3$, and CTC increased the sensitivity of the AgNPs-CTC towards the Y^{3+} ions.

2.4. Instrumentation

X-ray photoelectron spectroscopy (XPS) was performed on a Thermo Scientific (Theta Probe ARXPS), X-ray photoelectron spectrometer equipped with an Al K_α X-ray source to determine the chemical composition of the synthesized AgNPs-CTC. High-resolution transmission electron spectroscopy (HR-TEM) images of the AgNPs-CTC were collected using a JEOL JEM-2100 F before and after the AgNPs-CTC interacted with Y^{3+}. To investigate the coordination of the Y^{3+} with the AgNPs-CTC, energy-dispersive spectroscopy (EDS) elemental mapping was carried out using the JEOL JSM-2100 F electron microscope. X-ray diffraction (XRD) measurements were performed on a PANalytical X'Pert Pro diffractometer equipped with a Cu K_α radiation source ($\lambda = 1.5405$ Å); the scan speed was approximately 2°/min.

2.5. Sensing experiments

2.5.1. Determination of Y^{3+} ions

The colorimetric detection of Y^{3+} was carried out in aqueous solutions at ambient temperature (22 °C). In a typical measurement, the detection of Y^{3+} was carried out using the following procedure: AgNPs-CTC (50 µL) and different concentrations of Y^{3+} ions (from 18–243 nM) were added to water. After the coordination reaction was allowed to proceed for 10 min, the colorimetric changes were recorded using a UV–vis spectrophotometer. The corresponding color changes of the sensor solutions were photographed using a Samsung 8 + smartphone.

2.5.2. Effect of pH

The effect of pH values on the colorimetric detection performance was studied as follows: 50 µL of AgNPs–CTC stock solution was suspended in 0.85 mL of water in a UV–vis cuvette at different pH levels (2.1, 3.3, 4.1, 5.2, 6.0, 7.3, 8.2, and 9.3). The suspension was allowed to stand for 5 min, and the absorbance of the suspension was measured at 420 and 540 nm. Then, 100 µL of Y^{3+} (1.87 µM) was added. The reaction suspension was allowed to stand for another 5 min, and the absorbance of the suspension was again measured at 420 and 540 nm.

2.5.3. Time course of the AgNPs–CTC response toward Y^{3+}

The response time of AgNPs–CTC towards Y^{3+} was performed as follows: 50 µL of AgNPs–CTC stocking solution was suspended in 0.86 mL of water. The absorbance intensity was then measured. Subsequently, 90 µL of Y^{3+} (1.87 µM) was added to the aforementioned solution; the absorbance intensity was measured again at 420 and 540 nm every 60 s for 10 min.

2.5.4. Selectivity

To verify the selectivity of the CTC AgNP-based colorimetry, different metal cations (Y^{3+}, Zn^{2+}, Cd^{2+}, Cu^{2+}, Fe^{2+}, Fe^{3+}, Co^{2+}, Ba^{2+}, Se^{2+}, Hg^{2+}, Mn^{2+}, Cr^{3+}, Ca^{2+}, K^+, Bi^{3+}, Ge^{3+}, Pd^{2+}, Mo^{3+}, Pb^{2+}, Cs^+, Ni^{2+}, Zr^{4+}, As^{3+}, Mg^{2+}, and trivalent lanthanides including La^{3+}, Tb^{3+}, Sm^{3+}, Gd^{3+}, Pr^{3+}, Nd^{3+}, Dy^{3+}, Ho^{3+}, Er^{3+}, Tm^{3+}, Yb^{3+}, Ce^{3+}, Lu^{3+}, Eu^{3+}) and anions (PO_4^{3-}, NO_3–, and PO_4^{3-}), were tested in identical conditions. The selectivity of AgNPs–CTC towards Y^{3+} and lanthanides was confirmed as follows: 50 µL of AgNPs–CTC stock solution was suspended in 0.90 mL of water. And 50 µL of these above metal ions (1 ppm) was added and the UV–vis spectrums were recorded after 30 min.

2.5.5. Application to real water and serum samples

The real samples river water collected from the Han River and tap water collected from the laboratory were centrifuged at 14,000 rpm for 30 min, and the supernatant was used for analysis. Fetal bovine serum (Sigma-Aldrich, United States) was filtered through syringe filters with a 0.2 μm membrane. Afterward, the samples were stored in a refrigerator and then directly spiked with standard Y^{3+} solutions of different concentrations. These spiked samples were analyzed using the AgNPs–CTC solution and ICP-MS.

2.5.6. EDS/TEM analyses of Y^{3+}-induced AgNP-CTC aggregates

The AgNPs–CTC coordination reaction with Y^{3+} was performed as follows: 50 μL of AgNPs–CTC stock solution was suspended in 0.86 mL of nanopure water. Subsequently, 90 μL of Y^{3+} (1.87 μM) was added to the solution above. Afterward, 20 μL of the solution was carefully dropped onto carbon-coated copper grids, and the excess solution was removed with filter paper. EDS analysis was carried out to verify the adsorption of Y^{3+} ions onto the AgNPs–CTC surfaces. A transmission electron microscope (Jeol 2100 F) equipped with an EDS apparatus was used for imaging and elemental mapping of the obtained AgNPs–CTC aggregates.

2.6. Safety considerations

Because Y^{3+} ions are highly toxic, all trials involving Y^{3+} were performed with protective gloves. Experimental waste containing Y^{3+} ions was collected for proper disposal to avoid environmental contamination.

3. Results and discussion

3.1. Preparation of CTC-stabilized AgNPs

The temperature conditions of the AgNPs synthesis reaction can play an important role in determining the reaction rate, UV–vis spectral evolution patterns, and optical properties of the resultant AgNPs. To support this conclusion, the AgNPs synthesis experiments were performed in triplicate at different temperatures. The results of the trials are described to support the proposed premise. Before discussing the AgNPs synthesis results, we emphasize that an alkaline pH condition is necessary for the classical nucleation and growth route [12]. The synthesis reaction conducted near-neutral pH was too slow; thus, performing the reaction in the absence of an alkaline additive (NaOH) is not recommended. The reduction potential of CTC indicates that its reduction of Ag^{+} at room temperature is thermodynamically favorable. However, the formation of AgNPs was also investigated to optimize the productivity and reaction time of the AgNP synthesis at different temperatures during the reaction with CTC. Typically, 3 mL of CTC (3 mM) was added to 0.2 mL of NaOH (1 M) under static conditions, and the final volume of the reaction mixtures was subsequently brought to 4.8 mL using nanopure water. These reaction mixtures were incubated for 30 min at four different temperatures (20, 40, 60, and 80 °C); finally, 2 mL of $AgNO_3$ (20 mM) was mixed to initiate the synthesis of AgNPs at the respective temperature conditions. After a few minutes, the color of the reaction solution changed from colorless to yellow, indicating that the synthesis of AgNPs was initiated rapidly irrespective of the temperature. However, studying reaction rates is important in maximizing the yield and minimizing byproducts formation. This study intended to develop green synthesis method for of CTC functionalized AgNPs from $AgNO_3$ as a silver precursor and CTC as a reducing as well as a stabilizing agent [13].

The evolution of the UV–vis spectra of the AgNPs revealed two distinctly different pathways. The first pathway occurred at lower temperatures (20 and 40 °C) and involved linear increases in absorbance as a function of time. The second pathway occurred at higher temperatures (60 and 80 °C) and was responsible for an exponential increase in absorbance during the initial reaction period. UV–vis spectra of the reaction mixture incubated at 20 °C were recorded at different time intervals (Fig. S1a). The absorption data shown in Figure S1b indicate that a linear increase in absorbance occurred as a function of time from the early stage of synthesis for low-temperature condition 20 °C. Figure S1a,c shows UV–vis spectral patterns with a single narrow surface plasmon resonance (SPR) band even in the low-temperature condition (20 and 40 °C). For the reactions at 40 °C (Figure S4d), the linear increase in absorbance at 410 nm was consistent to 200 min. For the reactions at a higher temperature (60 °C), the absorbance at 410 nm increased rapidly within the first 20 min (Fig. S4e,f). Similarly, the AgNPs synthesis was most rapid at 80 °C, where the UV–vis absorbance at 410 nm emerged early during the reaction (5 to 10 min) (Figure S4g, bottom rows). As expected, the absorbance intensity of the AgNPs solution remained constant after substantial elongation of the incubation time, indicating high stability of the final product (Figure S4f,h). The temperature of the reaction mixture resulted in sharp UV–vis spectra; however, the UV–vis spectral evolution patterns and reaction rate successfully varied as a function of temperature [14]. Thus, data from this type of study may be valuable in optimizing the reaction conditions (e.g., temperature and time), mainly in future trials.

3.2. Characterization of AgNPs–CTC

AgNPs colloidal dispersions prepared at 80 °C for 300 min was further purified by ultracentrifugation at 12,000 rpm for 15 min. Dispersed AgNPs pellet in nanopure water was free from NaOH, $AgNO_3$, and CTC. XPS, TEM, and XRD were used to characterize the physicochemical properties of AgNPs, which were eventually used for the nanomolar-level detection of Y^{3+} ions in an aqueous environment. The surface chemical states and elemental composition of the AgNPs were analyzed using XPS, as shown in Figure S2. The survey spectrum indicated the presence of Ag3d, C1s, and O1s peaks (Fig. S2a), indicates resultant AgNPs were CTC functionalized. The Ag3d core spectrum was separated into two components, Ag $3d_{3/2}$ and Ag $3d_{5/2}$, centered at binding energies of 373.6 and 367.7 eV, respectively (Figure S2b). As shown in Figure S2c, the C1s core spectrum of the AgNP reveals a single major component at a binding energy of 284.5 eV, which is attributed to carbon atoms (CC− bonds) within the phenyl rings. The O1s high-resolution spectrum shows a single characteristic peak at 531.5 eV (Figure S2d), which represents C═O chemical structures.

Most of the AgNPs exhibit a spherical shape with a size ranging from 8 to 22 nm (Figure S3a). Figure S3a,b shows the TEM images of the AgNPs at two different magnifications. The selected area in Figure S3a is magnified and shown in Figure S3b. The AgNPs exhibited a crystalline nature, with lattice fringes displaying an interplanar distance of 0.26 nm (Fig. S3c). The chemical reduction reaction of CTC and silver salt exposed to high temperature resulted in well-dispersed spherical AgNPs with a homogenous shape and size. XRD patterns were recorded to identify the phase structure of the AgNPs (Figure S3d). The patterns of the AgNPs showed four 2θ peaks at 38.3°, 44.4°, 64.3°, and 77.1° corresponding to the (111), (200), (220), and (311) planes of cubic-phase Ag, respectively. The XRD and TEM analysis results confirmed the successful synthesis of crystalline AgNPs.

3.3. Interaction between Y^{3+} and AgNPs–CTC

The absorption spectra of the AgNPs–CTC in the presence of Y^{3+} at various concentrations were recorded. The absorption band of the AgNPs–CTC was very sensitive to the presence of target metal Y^{3+}. Thus, increase in the Y^{3+} concentration induced substantial changes in the absorption spectra of the AgNPs–CTC (Fig. 1a). The absorbance intensity of the SPR peak AgNPs–CTC decreased at 420 nm, and red-shifted peak increased at 540 nm in a linear fashion with increasing Y^{3+} concentration (Fig. 1b,c). Moreover, the color of the reaction solution changed from yellow to bright red as a result of the AgNPs–CTC

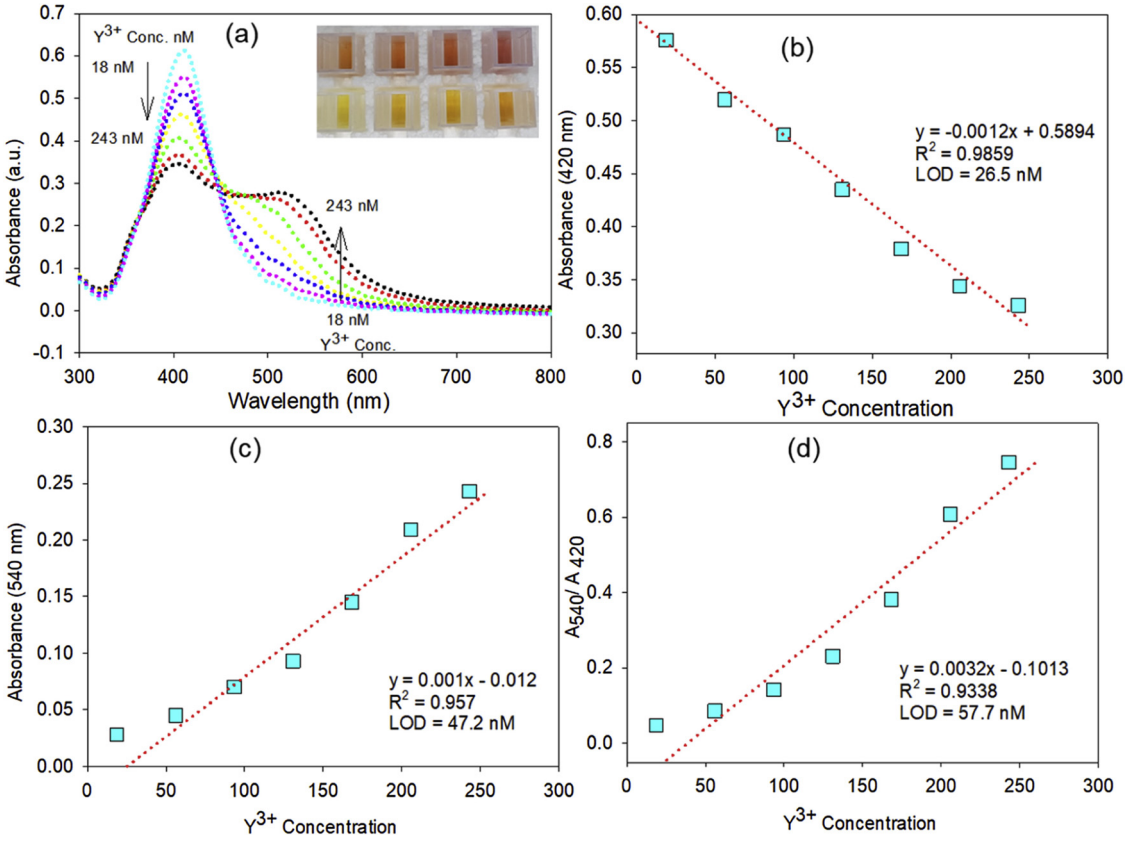

Fig. 1. (a) UV–vis spectra of AgNPs with increasing amounts of Y^{3+}. (b) Absorbance intensity (at 420 nm) with increasing amounts of Y^{3+} (inset image shows the colorimetric results). (c) Absorbance intensity (at 540 nm) with increasing amounts of Y^{3+} and ratiometric absorbance (A_{540nm}/A_{420nm}) with increasing amounts of Y^{3+}.

aggregation, as shown in the inset of Fig. 1b. We demonstrated the sensitivity of the AgNPs–CTC to nanomolar levels of Y^{3+} by monitoring the absorbance at 420 and 540 nm. Such probes based solely on absorbance intensity have achieved low detection limits but face challenges associated with quantifying Y^{3+} at higher concentrations. A ratiometric plot shows a linear pattern for Y^{3+} concentrations as high as 240 nM; however, higher Y^{3+} concentrations led to saturation behavior because of the limited number of O-containing moieties of CTC on AgNPs available to react with Y^{3+}. Taking advantage of SPR in developing ratiometric sensors for metal ions have drawn much attention because of their reliability and easy-to-differentiate color and intensity changes [15]. The color change was observed immediately after the AgNPs–CTC were exposed to different concentrations of Y^{3+}; the observed color change was easily discerned by the naked eye. Our AgNPs–CTC sensor exhibited better colorimetric performance concerning sensitivity, for absorbance response at 420 nm, 540, and ratiometric results LOD was about ˜26.5, 47.2, and 57.7 nM with R^2 = 0.985, 0.957, and 0.933, respectively (Fig. 1b-d). This probe can detect Y^{3+} ions at concentrations below the safe limit for drinking water and can thus function as a sensitive colorimetric indicator in practical sensing applications. The LOD of our proposed method is similar to or lower than those of other reported methods for detecting Y^{3+} ion (Table 1). The sensitivity of this colorimetric sensor was compared with those of other reported methods using various techniques [7,16,17].

CTC consists of multiple ionizable functional groups with a four-ring system. Thus, based on the spectral absorption positions, we investigated the direct binding of Y^{3+} to the AgNPs–CTC. We proposed that the added Y^{3+} to readily interact with the ligands of CTC and tend to form a stable complex with Y^{3+} because of the multiple O-containing moieties. Thus, it was thought that the CTC molecules act as a chelating agent to "capture" Y^{3+} ions, allowing them to form a stable coordination complex with AgNPs–CTC. Y^{3+} a rare-earth element; thus, complexation of Y^{3+} with CTC in water can yield a binary complex with a mole-ratio stoichiometry 1:1 of CTC to Y^{3+}. A plausible mechanism for the formation of AgNPs–CTC–Y^{3+} complex is presented in Fig. 2. The coordination number of Y^{3+} is normally 8, where the structure of the Y^{3+}–CTC forms a binary complex, in excellent agreement with the previously reported binary lanthanide–tetracycline complexes [18]. Notably, CTC molecules demonstrate excellent ability to adsorb Y^{3+} ions, mainly through O-containing moieties such as O–Y^{3+}–O as demonstrated in the previous report [11].

Table 1
Comparison of other methods and their sensitivities for Y^{3+} determination.

Method	Range	LOD	Reference
Fluorimetric	0–40 μM	5 μM	[7]
Fluorimetric	0–40 μM	5 μM	[27]
Fluorimetric	–	300 ppb	[28]
Spectrophotometric	0 to 50 ppm	1 ppm	[29]
Fluorimetric	75–600 ppb	100 ppb	[30]
Fluorimetric	–	0.013 ppb	[8]
Spectrophotometric	18–243 nM	57.7 nM	This study

3.4. Effect of pH

Typically, the pH values of a colorimetric probe solution strongly influence on the detection of the target metal ions. We, therefore, investigated the Y^{3+}-sensing ability of the AgNPs–CTC at different pH levels. The absorbance results recorded at 420 nm showed that the AgNPs–CTC was stable in the pH range from 5.2 to 9.3 and that their

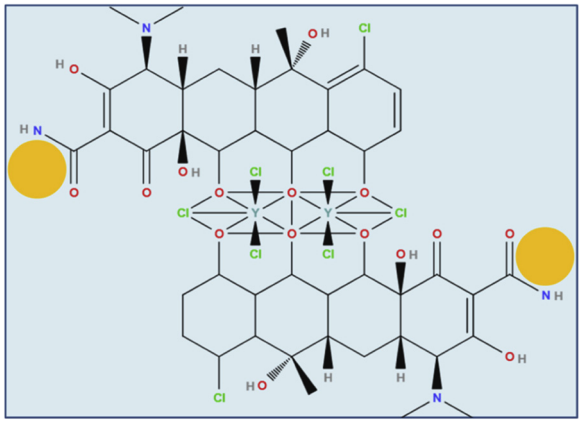

Fig. 2. Schematic illustration of coordination complex between AgNP-CTC and Y^{3+} ions.

response toward Y^{3+} was maximal at pH 7.3 (Fig. 3a). The results recorded at 540 nm also show that the AgNPs–CTC was stable within the pH range from 5.2 to 9.3 and that their response toward Y^{3+} was maximal at pH 7.3 (Fig. 3b). Therefore, we selected the nanopure water samples as the analytical condition for the detection and adsorptive removal of Y^{3+}. The effect of pH on the stability and the optical properties of CTC-functionalized AgNPs are in agreement with cysteine-functionalized AgNPs [19].

3.5. Time course of the AgNPs–CTC response toward Y^{3+}

Fig. 3c presents the response time recorded for the AgNPs–CTC towards the Y^{3+}. As noticed, the absorbance intensity at 420 nm decreased rapidly within 60 s. Initially, the absorbance intensity decreased to its minimum and then achieved a stable sensing platform. Fig. 3d presents a similar response time recorded at the red-shifted wavelength of 540 nm for AgNPs–CTC toward Y^{3+}. The absorbance intensity at 540 nm increased rapidly within 60 s. Irrespective of the initial Y^{3+} concentration, the response time was found to be 60 s for the AgNPs–CTC. Therefore, the absorbance probe could be realized at two different wavelengths for the rapid detection of Y^{3+} in the water samples. Due to its adverse effects, the development of a rapid and simple method for of Y^{3+} detection is vital as suggested previously for Ag^{+} ions [20].

3.6. Selectivity

In recent years, radioactive yttrium and lanthanide coordination with biomolecules and metal NPs have aroused tremendous interest for their optical properties and unique structural. However construction of metal NPs-based colorimetric probe for detection still remains a great challenge. Selectivity is an important parameter for the development of a practically viable sensor [21]. Therefore, the absorbance response of the AgNPs–CTC was examined using various metal ions (Zn^{2+}, Cd^{2+}, Cu^{2+}, Fe^{2+}, Fe^{3+}, Co^{2+}, Ba^{2+}, Se^{2+}, Hg^{2+}, Mn^{2+}, Cr^{3+}, Ca^{2+}, K^{+}, Bi^{3+}, Ge^{3+}, Pd^{2+}, Mo^{3+}, Pb^{2+}, Cs^{+}, Ni^{2+}, Zr^{4+}, As^{3+}, Mg^{2+}, and trivalent lanthanides, including La^{3+}, Tb^{3+}, Sm^{3+}, Gd^{3+}, Pr^{3+}, Nd^{3+}, Dy^{3+}, Ho^{3+}, Er^{3+}, Tm^{3+}, Yb^{3+}, Ce^{3+}, Lu^{3+}, Eu^{3+}) and anions (PO_4^{3-},

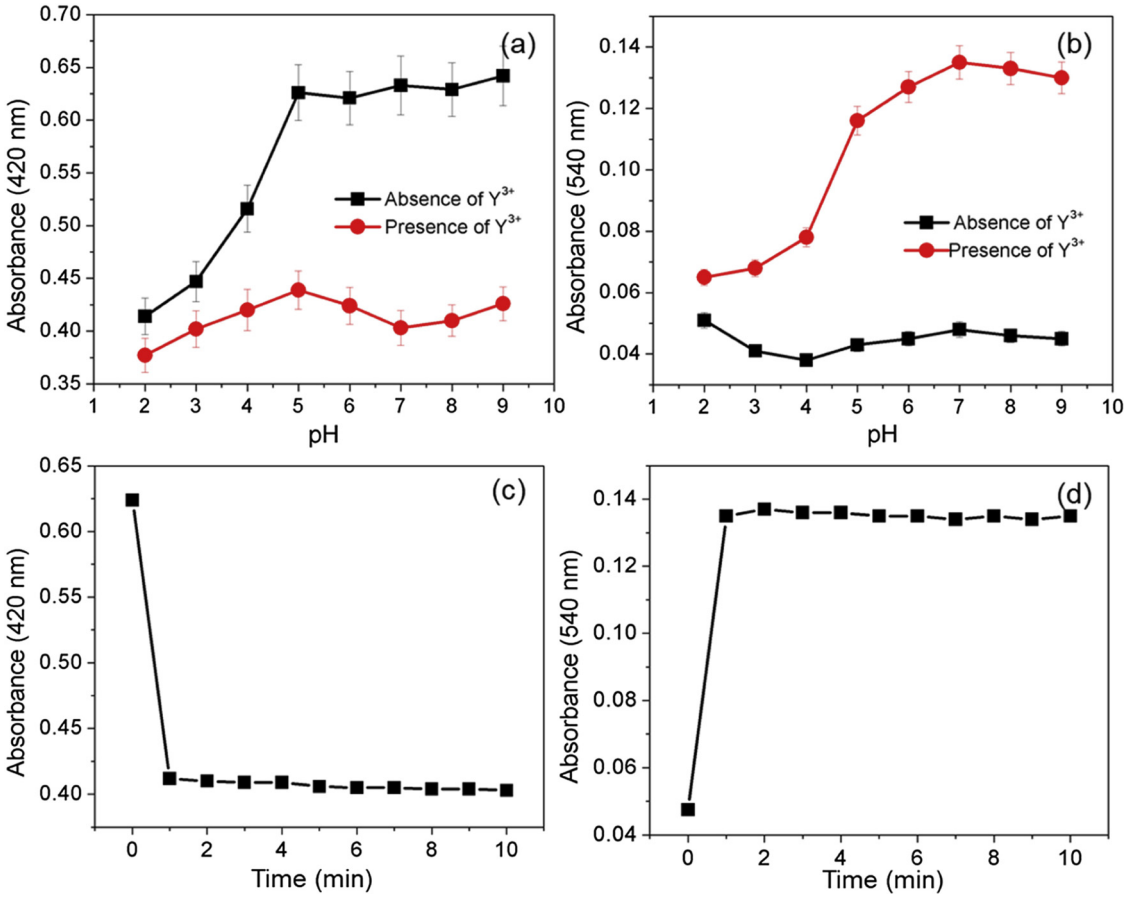

Fig. 3. (a) Absorbance intensity (420 nm) of AgNPs in the absence (black line) and presence (red line) of Y^{3+} at different pH. (b) Absorbance intensity (540 nm) of AgNPs in the absence (black line) and presence (red line) of Y^{3+} at different pH. (c) Time course of the absorbance response (420 nm) of AgNPs in the presence of Y^{3+} (200 nM) (For interpretation of the references to colour in this figure legend, the reader is referred to the web version of this article).

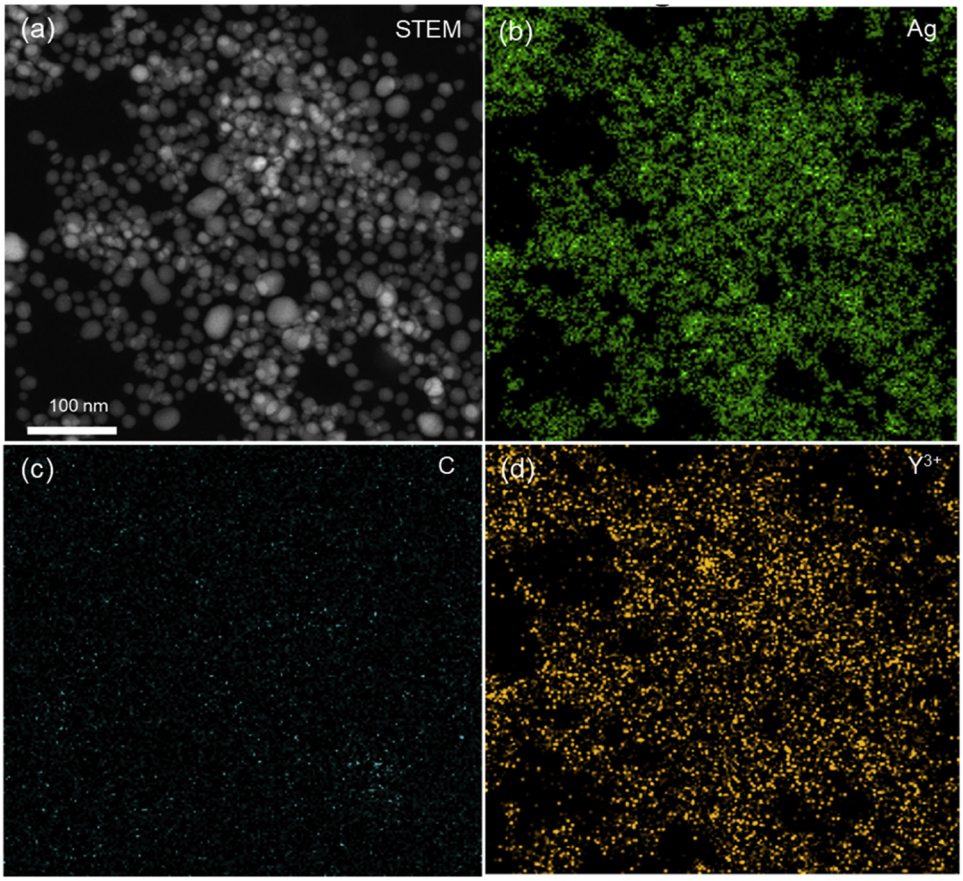

Fig. 4. (a) TEM image and energy dispersive X-ray (EDS) elemental mapping images of (b) Ag, (c) C, and (d) Y.

NO_3–, and PO_4^{3-}). The spectral results show that some of the other metal ions could enhance the absorbance intensity of the AgNPs–CTC Figure S4a-c. However, Y^{3+} could decrease the absorbance intensity at 420 nm with a red-shift of the AgNPs–CTC at 540 nm (Figure S4d-f). Similarly, AgNPs–CTC also found sensitive to the various trivalent lanthanides, where SPR absorbance intensity was significantly decreased as compared to the untreated AgNPs–CTC (Figure S4c). A red-shift towards larger wavelength was also observed for the range of lanthanides. Therefore, the developed method can be certainly applied in specific circumstances for Y^{3+} detection where yttrium compounds used exclusively or as a common colorimetric indicator for the detection of trace levels of Y^{3+} and lanthanides in the mixture. Since lanthanides and yttrium always coexist in spent nuclear fuels and in the mineral matrix, this method would be appropriate to express cautionary concerns over trace levels Y^{3+} and lanthanide metals.

3.7. EDS/TEM analysis results

Interestingly, a new peak at a longer wavelength of 540 nm was observed for Y^{3+} because of aggregation and agglomeration of AgNPs–CTC, as seen in the TEM image (Fig. 4a). EDS analysis has been conducted to verify the uptake of Y^{3+} ions in the AgNPs–CTC. Fig. 4 presents the EDS mapping results for Ag and Y^{3+} over aggregates of AgNPs–CTC. The Ag signal in an individual AgNPs–CTC is relatively uniform for AgNPs–CTC aggregates (Fig. 4a,b). However, the ubiquity of the distribution of carbon suggested that the carbon signals originated from the carbon-coated copper grids (Fig. 4c). The observed EDS signal of Y indicates that Y^{3+} ions are indeed adsorbed onto the AgNPs–CTC (Fig. 4d). The overlap results of the EDS images for two elements further confirm that all the AgNPs–CTC samples are capable of adsorbing Y^{3+} ions (Fig. 4b,d). The spatial distribution of the Y signal on an individual AgNPs–CTC is relatively uniform, implying that Y^{3+} ions efficiently adsorbs onto the interconnected CTC aggregates in the AgNPs in addition to adsorbing onto the dispersed AgNPs–CTC surfaces (Fig. 4b,d). These results indicate that CTC can be successfully used as a radioisotope-binding material and for removing Y^{3+} ions from water samples.

The presence of radioactive substances such as Y^{3+} in water poses a serious health hazard to the public; thus, new radioisotope-binding materials are needed [22]. In the present study, the Y^{3+}-binding activity of CTC was investigated in a batch adsorption process and demonstrated heavy adsorption of Y^{3+} onto AgNPs–CTC. The AgNPs–CTC with adsorbed Y^{3+} was easily collected by centrifugation to achieve the removal of Y^{3+} at low concentrations from contaminated water. The results show that the AgNPs–CTC act as an effective adsorbent for binding Y^{3+} in aqueous solutions, thus detection and remediation of Y^{3+}. *Streptomyces albus* was used to accumulate rare earth elements from a solution containing yttrium other heavy metals [23]. The removal of Y^{3+} ions from water samples using alginate compounds has been previously reported, where stable complexes were achieved with Y^{3+} ions [24].

3.8. Detection of Y^{3+} in real water samples

Y^{3+} is a heavy rare-earth element that has been widely used in various modern industrial processes, including the production of alloys, optical glasses, ceramics, and nuclear energy [25]. However, recently, high levels of Y contamination were detected in urine and drinking water near mining areas. Long-term exposure to Y^{3+} can severely affect human health and deserves serious attention [26]. To check the practical applicability of our colorimetric method, the AgNPs–CTC was tested on real samples. The Y^{3+} contamination levels in the real

Table 2
Determination of Y^{3+} contents in real water samples.

Real Samples	Added (nM)	ICP-MS (nM)	AgNPs-CTC (nM)	Recovery (%)	Relative error (%)
Fetal bovine serum	100	98 ± 3.8	96 ± 4.4	97.9	4.7
	50	53 ± 2.8	48 ± 2.9	90.5	7.8
	25	24 ± 1.4	26 ± 1.8	108.3	9.8
Tap water	100	97 ± 4.1	103 ± 3.8	106.1	8.9
	50	49 ± 2.7	53 ± 3.2	108.1	8.7
	25	26 ± 2.4	24 ± 2.3	92.3	6.8
River water	100	97 ± 4.4	102 ± 5.3	105.1	5.6
	50	52 ± 3.1	54 ± 3.7	103.8	8.4
	25	26 ± 2.4	28 ± 2.9	107.6	7.9

samples were below, approximately equal to, and higher than the LOD (25, 50, and 100 nM) of the developed sensor (Table 2). The identical colorimetric response towards pure water and real water samples suggest that the AgNPs–CTC were robust against interference from contaminants present in real water samples. Therefore, these results confirm the usefulness of the developed probe for the detection of Y^{3+} ions in real water samples. The short response time (within 1 min), lower detection limit at the nanomolar level, operation at physiological pH (pH 7.3), and applicability to real water samples makes our probe advantageous over other methods. The AgNPs–CTC sensor used for the determination of Y^{3+} in spiked samples such as real water samples from different sources and fetal bovine serum led to useful and reasonable results, as suggested in a previous report [16].

4. Conclusions

In conclusion, novel CTC-modified AgNPs were synthesized, characterized, and used to detect the toxic Y^{3+} ions. The absorance signals from aggregation state of AgNPs-CTC were appeared immediately after coordination with Y^{3+} and lanthanides on the surface, which enables to detected target analytes by naked-eyes. The bonding of the O-containing moieties of CTC with Y^{3+} led to absorbance changes of the AgNPs–CTC, making them useful as a highly sensitive sensor. The colorimetric detection method is based on the fact that the AgNPs–CTC undergoes aggregation because of the formation of a chelating complex between Y^{3+} ions and O–groups. The systematic performance of Y^{3+} sensor based on the AgNPs–CTC was examined by colorimetric and spectrophotometric techniques and was found to be reliable in terms of response time, sensitivity, LOD, and reproducibility. This colorimetric method can be introduced as a novel approach to provide cautionary measures for Y^{3+} and lanthanides in environmental samples. This study can guide to fabricate portable vials and test strips for easy and on-site detection of Y^{3+} and lanthanides up to nanomolar level.

Acknowledgments

This work was supported by the Dongguk University Research Fund of 2018–2020

Appendix A. Supplementary data

Supplementary material related to this article can be found, in the online version, at doi:https://doi.org/10.1016/j.colsurfb.2019.110436.

References

[1] M.L. Dietz, E.P. Horwitz, Improved chemistry for the production of yttrium-90 for medical applications, Appl. Radiat. Isot. 43 (1992) 1093–1101.
[2] C.-H. Yeong, M.-H. Cheng, K.-H. NG, Therapeutic radionuclides in nuclear medicine: current and future prospects, J. Zhejiang Univ. Sci. B 15 (2014) 845–863.
[3] C.R. Cánovas, F. Macías, R. Pérez López, J.M. Nieto, Mobility of rare earth elements, yttrium and scandium from a phosphogypsum stack: environmental and economic implications, Sci. Total Environ. 618 (2018) 847–857.
[4] C.E. Lisowski, J.E. Hutchison, Malonamide-functionalized gold nanoparticles for selective, colorimetric sensing of trivalent lanthanide ions, Anal. Chem. 81 (2009) 10246–10253.
[5] E.S. Koshel', V.B. Baranovskaya, T.Y. Gubanova, Direct arc atomic emission analysis of yttrium, gadolinium, and neodymium oxides, Inorg. Mater. Appl. Res. 52 (2016) 1449–1454.
[6] Z. Zhu, A. Zheng, Fast determination of yttrium and rare earth elements in seawater by inductively coupled plasma-mass spectrometry after online flow injection pretreatment, Molecules 23 (2018) 489.
[7] K. Okamoto, S. Fukuzumi, An yttrium ion-selective fluorescence sensor based on metal ion-controlled photoinduced electron transfer in zinc porphyrin – quinone dyad, J. Am. Chem. Soc. 126 (2004) 13922–13923.
[8] D. Zhang, Z. Zang, X. Zhou, Y. Zhou, X. Tang, R. Wei, W. Liu, A selective fluorescence probe for yttrium(III) based on acylhydrazone Schiff base, Inorg. Chem. Comm. 12 (2009) 1154–1156.
[9] V. Minganti, G. Drava, Tree bark as a bioindicator of the presence of scandium, yttrium and lanthanum in urban environments, Chemosphere 193 (2018) 847–851.
[10] K.D. Mjos, C. Orvig, Metallodrugs in medicinal inorganic chemistry, Chem. Rev. 114 (2014) 4540–4563.
[11] W. Thanasarakhan, S. Kruanetr, R.L. Deming, B. Liawruangrath, S. Wangkarn, S. Liawruangrath, Sequential injection spectrophotometric determination of tetracycline antibiotics in pharmaceutical preparations and their residues in honey and milk samples using yttrium (III) and cationic surfactant, Talanta 84 (2011) 1401–1409.
[12] D.-Y. Kim, M. Kim, S. Shinde, R.G. Saratale, J.-S. Sung, G. Ghodake, Temperature dependent synthesis of tryptophan-functionalized gold nanoparticles and their application in imaging human neuronal cells, ACS Sustain. Chem. Eng. 5 (2017) 7678–7689.
[13] F.K. Alsammarraie, W. Wang, P. Zhou, A. Mustapha, M. Lin, Green synthesis of silver nanoparticles using turmeric extracts and investigation of their antibacterial activities, Colloids Surf. B Biointerfaces 171 (2018) 398–405.
[14] X.C. Jiang, W.M. Chen, C.Y. Chen, S.X. Xiong, A.B. Yu, Role of temperature in the growth of silver nanoparticles through a synergetic reduction approach, Nanoscale Res. Lett. 6 (2010) 32–32.
[15] D.-M. Chen, C.-X. Sun, Y. Peng, N.-N. Zhang, H.-H. Si, C.-S. Liu, M. Du, Ratiometric fluorescence sensing and colorimetric decoding methanol by a bimetallic lanthanide-organic framework, Sensor Actuat B: Chem. 265 (2018) 104–109.
[16] M.M. Hussain, M.M. Rahman, M.N. Arshad, A.M. Asiri, Trivalent Y3+ ionic sensor development based on (E)-Methyl-N′-nitrobenzylidene-benzenesulfonohydrazide (MNBBSH) derivatives modified with nafion matrix, Sci. Rep. 7 (2017) 5832.
[17] K.V. Zhernokleeva, V.B. Baranovskaya, Analysis of pure scandium, yttrium, and their oxides using methods of inductively coupled plasma atomic emission spectrometry and inductively coupled plasma mass spectrometry, Inorg. Mater. Appl. Res. 47 (2011) 1627–1634.
[18] G. Karthikeyan, K. Mohanraj, K.P. Elango, K. Girishkumar, Synthesis, spectroscopic characterization and antibacterial activity of lanthanide–tetracycline complexes, Transit. Metal Chem. 29 (2004) 86–90.
[19] E. Csapó, R. Patakfalvi, V. Hornok, L.T. Tóth, Á. Sipos, A. Szalai, M. Csete, I. Dékány, Effect of pH on stability and plasmonic properties of cysteine-functionalized silver nanoparticle dispersion, Colloids Surf. B Biointerfaces 98 (2012) 43–49.
[20] G. Wang, S. Wang, C. Yan, G. Bai, Y. Liu, DNA-functionalized gold nanoparticle-based fluorescence polarization for the sensitive detection of silver ions, Colloids Surf. B Biointerfaces 167 (2018) 150–155.
[21] R.G. Saratale, G.D. Saratale, G. Ghodake, S.-K. Cho, A. Kadam, G. Kumar, B.-H. Jeon, D. Pant, A. Bhatnagar, H.S. Shin, Wheat straw extracted lignin in silver nanoparticles synthesis: expanding its prophecy towards antineoplastic potency and hydrogen peroxide sensing ability, Int. J. Biol. Macromol. 128 (2019) 391–400.
[22] L. Domínguez-Gadea, L. Cerezo, Decontamination of radioisotopes, Rep. Pract. Oncol. Radiother. 16 (2011) 147–152.
[23] T. Tsuruta, Selective accumulation of light or heavy rare earth elements using gram-positive bacteria, Colloids Surf. B Biointerfaces 52 (2006) 117–122.
[24] M. Khotimchenko, V. Kovalev, E. Khozhaenko, R. Khotimchenko, Removal of yttrium (III) ions from water solutions by alginate compounds, Int. J. Environ. Sci. Technol. 12 (2015) 3107–3116.
[25] A.V. Naumov, Review of the world market of rare-earth metals, Russ. J. Non-Ferr. Met. 49 (2008) 14–22.
[26] Q. Liang, H. Yin, J. Li, L. Zhang, R. Hou, S. Wang, Investigation of rare earth elements in urine and drinking water of children in mining area, Medicine 97 (2018) e12717.
[27] J.-M. Liu, C.-F. Chen, Q.-Y. Zheng, Z.-T. Huang, A selective fluorescent probe for La3+ and Y^{3+} based on calix[6]arene, Tetrahedron Lett. 45 (2004) 6071–6074.
[28] M. Shen, C.M. Li, D. Na, Z.Q. Hao, X.Y. Li, L.B. Guo, Y.F. Lu, X.Y. Zeng, Determination of yttrium in titanium alloys using laser-induced breakdown spectroscopy assisted with laser-induced fluorescence, J. Anal. Atom. Spectrom. 33 (2018) 658–662.
[29] D.F. Wood, M.R. Adams, Spectrophotometric determination of yttrium in chromium and chromium-base alloys with arsenazo III, Analyst 95 (1970) 556–561.
[30] J.M.C. Pavón, M.E.U. Pozo, A.G. de Torres, C.B. Ojeda, Fluorimetric determination of trace amounts of yttrium with salicylaldehyde carbohydrazone, Analyst 113 (1988) 1291–1294.